loss of ~18% of current atmospheric oxygen during 3 Gy, does not represent the net atmospheric oxygen loss from Earth. In other words, the net loss can be one order of magnitude smaller than the polar outflow rate; i.e., less than 2% of atmospheric oxygen has been lost over 3 Gy. The result also suggests that the current oxygen loss rate from Earth is almost one order smaller than that from Mars (30×10^{24} ions s^{-1}) (*15*) and Venus (50×10^{24} ions s^{-1}) (*16*). It might indicate that the existence of a substantial intrinsic magnetic field can help a planet to keep its atmosphere. Alternatively, the resultant one order difference between estimates of the polar outflow and the four routes might indicate the existence of unknown loss processes for terrestrial oxygen. One possibility is the escape of cold O^+ ions at energies below 50 eV either to the magnetosheath or through the plasma sheet, which are difficult to observe in the magnetosphere without spacecraft potential control. Another candidate may be the charge exchange loss of ring current ions (*17*) that become dominated by O^+ during magnetic storm periods. For further understanding, systematic ion-composition measurements in the magnetosheath and the plasma sheet as well as quantitative investigation of ring current loss mechanisms are needed.

References and Notes

1. B. D. Shizgal, G. G. Arkos, *Rev. Geophys.* **34**, 483 (1996).
2. A. W. Yau, W. K. Peterson, E. G. Shelley, in *Modeling Magnetospheric Plasma*, T. E. Moore, J. H. Waite Jr., Eds., *Geophysical Monogr. Ser.*, vol. 44 (American Geophysical Union, Washington, DC, 1988), pp. 211–217.
3. A. W. Yau, M. André, *Space Sci. Rev.* **80**, 1 (1997).
4. K. Seki *et al.*, *J. Geophys. Res.* **103**, 4477 (1998).
5. M. Hirahara *et al.*, *J. Geophys. Res.* **101**, 7769 (1996).
6. K. Seki *et al.*, *J. Geophys. Res.* **105**, 15931 (2000).
7. A. Nishida, T. Mukai, T. Yamamoto, S. Kokubun, K. Maezawa, *J. Geophys. Res.* **103**, 4409 (1998).
8. T. Yamamoto, K. Shiokawa, S. Kokubun, *Geophys. Res. Lett.* **21**, 2875 (1994).
9. D. T. Young, H. Balsiger, J. Geiss, *J. Geophys. Res.* **87**, 9077 (1982).
10. A. Ieda *et al.*, *J. Geophys. Res.* **103**, 4453 (1998).
11. W. Lennartsson, *J. Geophys. Res.* **94**, 3600 (1989).
12. S. A. Fuselier, D. M. Klumpar, E. G. Shelley, *J. Geophys. Res.* **96**, 47 (1991).
13. T. D. Phan *et al.*, *Nature* **404**, 848 (2000).
14. Q.-W. Zong, B. Wilken, *Geophys. Res. Lett.* **26**, 3349 (1999).
15. R. Lundin *et al.*, *Nature* **341**, 609 (1989).
16. L. H. Brace *et al.*, *J. Geophys. Res.* **92**, 15 (1987).
17. E. C. Roelof, *Adv. Space Res.* **20**, 361 (1997).
18. We thank all GEOTAIL science members for their collaboration. This work was carried out under the auspices of the Research Fellowships of the Japan Society for the Promotion of Science for Young Scientists.

Quantum Mechanical Actuation of Microelectromechanical Systems by the Casimir Force

H. B. Chan, V. A. Aksyuk, R. N. Kleiman, D. J. Bishop, Federico Capasso*

The Casimir force is the attraction between uncharged metallic surfaces as a result of quantum mechanical vacuum fluctuations of the electromagnetic field. We demonstrate the Casimir effect in microelectromechanical systems using a micromachined torsional device. Attraction between a polysilicon plate and a spherical metallic surface results in a torque that rotates the plate about two thin torsional rods. The dependence of the rotation angle on the separation between the surfaces is in agreement with calculations of the Casimir force. Our results show that quantum electrodynamical effects play a significant role in such microelectromechanical systems when the separation between components is in the nanometer range.

Microelectromechanical systems (MEMS) are movable structures fabricated on a semiconductor wafer through the use of integrated circuits technology (*1*) and have become a key technology in the production of sensors and actuators. So far, the smallest separations between surfaces of micromachined components are typically on the order of micrometers, and the operation of MEMS is well described by classical mechanics. As further miniaturization takes place, quantum effects may become significant in device design and operation (*2*). The Casimir effect (*3–7*), for example, is the attractive force between two uncharged conducting surfaces, arising from quantum fluctuations of the electromagnetic field. According to quantum theory, electro-magnetic fields fluctuate and therefore can never be exactly zero. This gives rise to a finite zero point energy even when there are no photons in the field. In the presence of two perfectly conducting plates, the electromagnetic field must satisfy the boundary conditions. The zero point energy density of the electromagnetic field between the conducting plates is lower than in free space. As a result, there is a net attractive force per unit area between the plates, given by (*3*)

$$F_c = -\frac{\pi^2 \hbar c}{240} \frac{1}{z^4} \qquad (1)$$

where c is the speed of light, $\hbar$ is Planck constant/2π, and z is the separation between the plates. When the separation between the surfaces decreases, the Casimir pressure increases rapidly, reaching about 1 atmosphere at $z \sim 10$ nm. Sparnaay (*8*) performed the first measurement that showed evidence for the Casimir force, but experimental uncertainties were too large for a quantitative verification of the effect. Recently, the Casimir force was accurately measured with the use of a torsional pendulum (*9*) and an atomic force microscope (*10*, *11*). In both cases, one of the surfaces was chosen to be spherical to avoid the problem of keeping two flat surfaces parallel. According to the proximity force theorem (*12*, *13*), this geometry modifies the Casimir force to

$$F_{cs} = -\frac{\pi^3 \hbar c}{360} R \frac{1}{z^3} \qquad (2)$$

where R is the radius of the spherical surface. These experiments generated renewed theoretical interest in the Casimir force, in particular the corrections due to nonideal experimental conditions such as surface roughness and finite conductivity (*14–19*).

We demonstrate the actuation of a micromachined torsional device by the Casimir force. Our device consists of a 3.5-μm-thick, 500-μm^2 heavily doped polysilicon plate freely suspended on two of its opposite sides by thin torsional rods (Fig. 1A). The other ends of the torsional rods are anchored to the substrate by support posts (Fig. 1B). Two fixed polysilicon electrodes (not visible in Fig. 1A) are located symmetrically underneath the plate, one on each side of the torsional rod. Each electrode is half the size of the top plate. There is a 2-μm gap between the top plate and the fixed electrodes created by etching a SiO_2 sacrificial layer. The top plate is thus free to rotate about the torsional rods in response to an external torque.

To detect rotation of the plate, we measure the capacitance between the top plate and the bottom electrodes. In the absence of an external torque, the capacitances of the top plate to each electrode are almost equal. When an external torque tilts the top plate, one of the capacitances increases and the other one de-

Bell Laboratories, Lucent Technologies, Murray Hill, NJ 07974, USA.

*To whom correspondence should be addressed. E-mail: fc@lucent.com

creases. In demonstrating operation of the device (Fig. 1C), a dc voltage is applied to the electrode on the right to electrostatically attract and tilt the top plate while a small ac excitation (100 mV) is used to measure the capacitance between the top plate and the other electrode. The capacitance decreases as the plate moves further apart from the sensing electrode. At 0.16 V, the top plate tilts so much that it becomes unstable and snaps down to the electrode on the right (20). As the dc voltage is further increased, the capacitance stays constant because the top plate cannot tilt any further. When the dc voltage is swept back down, the top plate remains stuck to the electrode. The restoring torque from the torsional rods is not sufficient to pull the top plate back up. It is possible to free a stuck top plate by poking on it with a sharp tip or by applying voltage pulses to the electrodes.

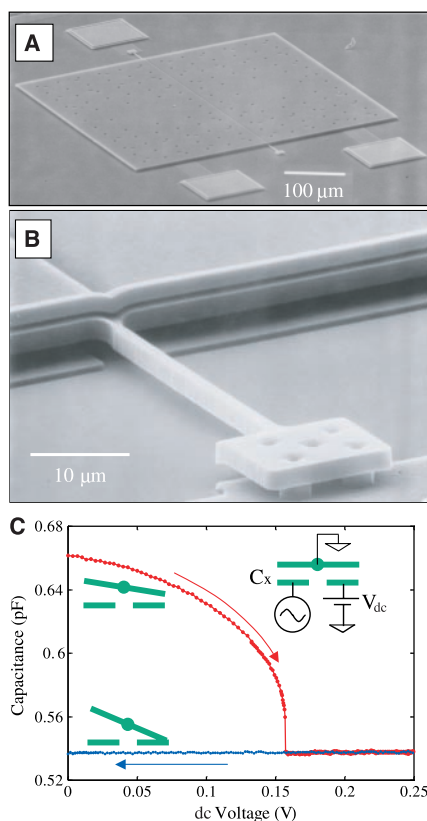A bridge circuit (21) enables us to measure

the change in capacitance to 1 part in 2×10^5, equivalent to a rotation angle of 8×10^{-8} rad, with an integration time of 1 s when the device is in a vacuum. With a torsional spring constant as small as 1.5×10^{-8} Nm rad^{-1}, the device yields a sensitivity of 5 pN Hz$^{-1/2}$ for forces acting at the edge of the plate. Such force sensitivity is comparable to the resolution of conventional atomic force microscopes. Despite the soft torsional spring constant, the device is insensitive to mechanical noise from the surroundings because the resonant frequency is maintained high enough ($\sim$2 kHz) owing to the small moment of inertia of the plate.

A schematic of the experimental setup to actuate the top plate of the device by means of the Casimir force is shown in Fig. 2 (inset). A polystyrene sphere with radius $R = 100$ μm is glued onto the end of a copper wire with conductive epoxy. A 200-nm-thick film of gold with a thin chromium adhesion layer is then evaporated on both the sphere and the top plate of the device. An additional 10-nm layer of gold is sputtered onto the sphere to provide electrical contact to the wire. The micromachined device is placed on a piezoelectric translation stage with the sphere positioned close to one side of the top plate. As the piezo extends, it moves the micromachined device toward the sphere. By measuring the difference in the capacitance of the top plate to the two bottom electrodes, we deduce the rotation of the top plate in response to the attractive force at different separations between the sphere and the top plate. The measurement is performed at room temperature and at a pressure of less than 1 mtorr.

The torsional rods provide the restoring torque to counter the external torque on the top plate. According to Hooke's law, the restoring torque τ is proportional to the rotation angle θ:

$$\tau = -k_1\theta \tag{3}$$

For the measurements described below, the rotation of the top plate is small so that the capacitance between the top and bottom electrodes deviates by less than 0.5% from the

unperturbed value. In this small signal regime, the rotation θ of the top plate depends linearly on the change in capacitance ΔC:

$$\theta = a\Delta C \tag{4}$$

From the geometry and dimensions of the device, the proportionality constant a is determined to be 0.0267 rad pF^{-1}. By equating the restoring torque of the torsional rods and the torque produced by the attractive force F between the top plate and the sphere, we obtain the following relations:

$$bF = k_1\theta \tag{5}$$

$$F = \alpha\theta \tag{6}$$

where $\alpha = k_1/b$ and b is the lateral distance of the center of the sphere from the torsional axis. We calibrate the proportionality constant α by measuring the electrostatic attraction as a function of separation between the sphere and the plate. A dc voltage is applied to the sphere while the electrostatic potential of the top plate is maintained at 0 V through the virtual ground of a preamplifier (21). The electrostatic force F_e between the sphere and the top plate is given by

$$F_e = -\varepsilon_o\pi R \frac{(V - V_o)^2}{z + z_o} \quad \text{for } z + z_o \ll R \tag{7}$$

where ε_o is the permittivity of vacuum, R is the radius of the sphere, V is the voltage applied to the sphere, V_o is the residual voltage on the sphere, z_o is the distance of closest approach of the sphere, and z is the separation between the sphere and plate measured from the position of closest approach. The closed-loop piezoelectric stage provides accurate and reproducible changes in z. In the calculation of z, a small correction due to the tilt of the top plate in response to the external force is taken into account (22). The distance of closest approach z_o is nonzero as a result of both surface roughness and mechanical instability. If the sphere approaches the plate beyond z_o, the plate becomes unstable and jumps into contact with the sphere. A fit of the measured tilt angle is shown (Fig. 2) in
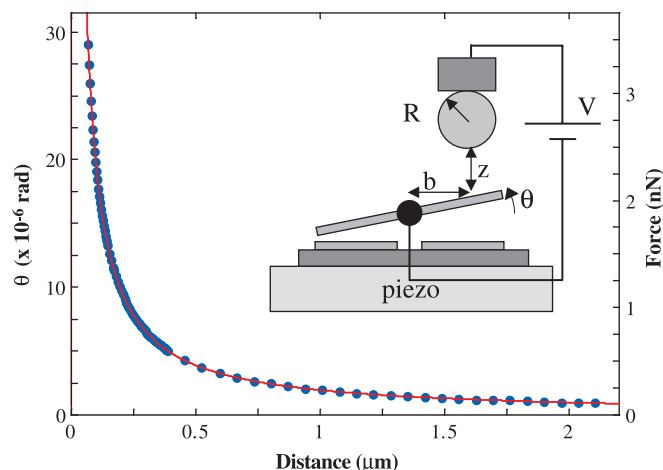
Fig. 1. Scanning electron micrographs of (**A**) the micromachined torsional device and (**B**) a close-up of one of the torsional rods anchored to the substrate. The fixed electrodes are connected by polysilicon lines to the two wire-bonding pads at the bottom of (A), whereas the top plate is connected by one of the torsional rods to the bond pad at the top of (A). (**C**) The capacitance C_x between the top plate and the left electrode as a function of dc voltage V_{dc} applied to the electrode on the right. The inset (top right) is a cross-section schematic of the device (not to scale) with the electrical connections.

Fig. 2. Angle of rotation θ of the top plate and the attractive electrostatic force as a function of distance (23). The red line is a fit obtained with Eq. 7. The voltage V applied to the sphere is 289 mV. (Inset) Schematic of the experiment (not to scale).

response to the electrostatic force (23) as a function of distance with Eqs. 6 and 7, with α and z_o as fitting parameters. The fitted values of α and z_o are 5.97×10^{-5} N rad^{-1} and 67.0 nm, respectively.

In Eq. 7, the residual voltage V_o arises from the work function difference of the two gold surfaces (the sphere and the top plate) as a result of slight variations in the preparation of the films. V_o is found to be 30 mV by fixing the distance z and identifying the voltage V at which the minimum of the quadratic voltage dependence of the force occurs.

To demonstrate actuation of the top plate by the Casimir force, we set the voltage V on the sphere equal to the residual voltage V_o to eliminate the electrostatic contributions to the attractive force. We then repeat the measurement by extending the piezoelectric stage so that the sphere approaches the plate. At distances greater than 300 nm, there is no detectable tilt of the top plate owing to negligible attraction between the two surfaces (Fig. 3A). When the sphere is within 300 nm of the plate, the attractive force increases rapidly and the top plate tilts by an angle of 6 µrad at the closest approach of 75.7 nm. The sharp rise of the force is distinct from the inverse distance dependence given by Eq. 7 that is characteristic of electrostatic attractions (shown as a green line in Fig. 3A).

The simple formula for the Casimir force in Eq. 2 is valid when the surfaces are smooth and perfectly reflecting at all frequencies. To compare the experimental data to theory, one must take into account two significant modifications to the Casimir force. First, there are modifications arising from the finite conductivity of the metal films at high frequencies. In the simplest case, that of the free-electron model, metals become transparent above the plasma frequency. The optical absorption of real metals departs from the free-electron model when the actual band structure is taken into account. For gold, the reflectance drops to 50% at a wavelength of ~500 nm (24). The gold surfaces in our experiment are therefore not as effective in confining the electromagnetic modes at short wavelengths. Because the major contribution to the Casimir force comes from the electromagnetic modes with wavelength comparable to the separation between the surfaces, the Casimir force between the gold surfaces is weaker than the idealized case at small separations (<500 nm). Lifshitz (25) incorporated the finite conductivity modifications to the Casimir force on the basis of the frequency dependence of the dielectric function of the metal. The attractive force between a sphere and a flat surface can be calculated numerically with the tabulated complex dielectric function of gold (18, 19):

$$F_1(z) = \frac{\hbar}{2\pi c^2} R \int\limits_0^\infty \int\limits_1^\infty$$
$$\times p\xi^2 \left\{ \log\left[1 - \frac{(s-p)^2}{(s+p)^2} e^{-2pz\xi/c} \right] \right.$$
$$\left. + \log\left[1 - \frac{(s-p\varepsilon)^2}{(s+p\varepsilon)^2} e^{-2pz\xi/c} \right] \right\} dp\,d\xi \quad (8)$$

where $s = \sqrt{\varepsilon - 1 + p^2}$ and $\varepsilon(i\xi)$ is the dielectric function of gold evaluated with imaginary frequency $i\xi$.

The second modification, due to the roughness of the metallic surfaces, tends to increase the attraction (14, 15). It further modifies the Casimir force:

$$F_2(z) = F_1(z)\left[1 + 6\left(\frac{A_r}{z}\right)^2 + 15\left(\frac{A_r}{z}\right)^4 \right] \quad (9)$$

The roughness amplitude A_r of the gold films is 30 nm, as measured by an atomic force microscope on an area of 1 µm^2. F_2 gives the theoretical Casimir force between a spherical surface and a flat surface including corrections of both surface roughness and finite conductivity. In Fig. 3A, the red line is a least-squares fit of the experimental data with $F_2(z - z_1)$, in which z_1 is a fitting parameter. The fitted value of z_1 is 75.7 ± 1 nm, consistent with z_o obtained from electrostatic calibration (67.0 nm) to within the roughness of the surface. When a fitting range of 500 nm in distance is used, the root-mean-square (rms) deviation of experimental data from the theoretical Casimir force, including both the finite conductivity and surface roughness corrections, is 2.4 pN.
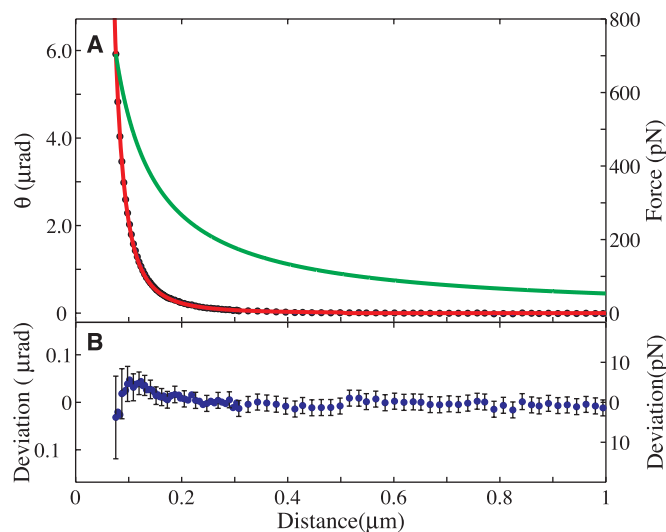
Even though the rms deviation between our experimental data and the theoretical result is less than 0.5% at the smallest separation, we do not claim agreement to the theory at the same level of precision. In calculating the finite conductivity corrections to the Casimir force, we used tabulated optical properties of gold. Because of variations in preparation techniques, it is unlikely that the optical properties of the gold films in our experiment agree with the tabulated values to better than 1%. As pointed out by Lamoreaux (26, 27), a fundamental test of the theory would require a direct measurement of the optical properties of the metal under study. In addition, the relatively large surface roughness complicates an exact comparison between data and theory (27). In Eq. 9, the expansion parameter A_r/z is about 0.4 at the smallest separation, resulting in surface roughness corrections of more than 50% of the net force. Corrections of such magnitude may introduce potential errors larger than 1% in the calculations. Therefore, verification of the theory of the Casimir force to better than 1% would require surfaces with improved roughness.

Nevertheless, the agreement between the measured tilt angle and theory shows unambiguously that the top plate of the torsional device is actuated solely by the Casimir force. We demonstrated that when the separation between surfaces is small, quantum effects must be considered to correctly describe the operation of our micromachined device. This could open new possibilities for novel actuation schemes in MEMS based on the Casimir force and may be important in the design of nanoelectromechanical systems (28).

Fig. 3. (A) Angle of rotation of the top plate in response to the Casimir force as a function of distance. The red line is a fit obtained with Eq. 9. For comparison, the electrostatic force (green, calculated with Eq. 7) has a much longer range. The voltage is chosen so that the electrostatic force equals the Casimir force at the point of closest approach. **(B)** Deviations of data in (A) from the fit of Casimir force. The vertical scale in (B) is a factor of 20 smaller than that of (A). The vertical bars represent the measurement uncertainties associated with the data in (A). Electrical noise of the amplifier results directly in uncertainties in the measured Casimir force and indirectly leads to uncertainties through errors in the proportionality constant α that is calibrated by fitting Eqs. 6 and 7 to the measured electrostatic force in Fig. 2.

References and Notes
1. W. S. Trimmer, *Micromechanics and MEMS: Classic and Seminal Papers to 1990* (IEEE Press, New York, NY, 1997).
2. F. M. Serry, D. Walliser, G. J. Maclay, *J. Microelectromech. Syst.* **4**, 193 (1995).

3. H. B. G. Casimir, *Proc. K. Ned. Akad. Wet.* **51**, 793, (1948).
4. E. Elizalde, A. Romeo, *Am. J. Phys.* **59**, 711 (1991).
5. P. W. Milonni, M. L. Shih, *Contemp. Phys.* **33**, 313 (1992).
6. L. Spruch, *Science* **272**, 1452 (1996).
7. M. Schaden, L. Spruch, *Phys. Rev. Lett.* **84**, 459 (2000).
8. M. J. Sparnaay, *Physica* **24**, 751 (1958).
9. S. K. Lamoreaux, *Phys. Rev. Lett.* **78**, 5 (1997).
10. U. Mohideen. A. Roy, *Phys. Rev. Lett.* **81**, 4549 (1998).
11. A. Roy, U. Mohideen, *Phys. Rev. Lett.* **82**, 4380 (1999).
12. B. V. Derjaguin, I. I. Abrikosova, E. M. Lifshitz, *Q. Rev. Chem. Soc.* **10**, 295 (1956).
13. J. Blocki, J. Randrup, W. J. Swiatecki, C. F. Tsang, *Ann. Phys.* **105**, 427 (1977).
14. A. A. Maradudin, P. Mazur, *Phys. Rev. B* **22**, 1677, (1980).
15. V. B. Bezerra, G. L. Klimchitskaya, C. Romero, *Mod. Phys. Lett. A* **12**, 2613 (1997).
16. J. Schwinger, L. L. DeRaad, K. A. Milton, *Ann. Phys.* **115**, 1 (1978).
17. M. Bordag, B. Geyer, G. L. Klimchitskaya, V. M. Mostepanenko, *Phys. Rev. D* **56**, 075003 (1998).
18. A. Lembrecht, S. Reynaud, *Eur. Phys. J. D* **8**, 309 (2000).
19. G. L. Klimchitskaya, U. Mohideen, V. M. Mostepanenko, *Phys. Rev. A* **61**, 062107 (2000).
20. The restoring torque of the torsional rod increases linearly with rotation angle, whereas the torque due to electrostatic attraction from the electrode is a strongly nonlinear function of the rotation angle. As the top plate rotates closer to the electrode, the electrostatic torque increases rapidly. As a result, once the angle of rotation exceeds a threshold value, the top plate becomes unstable and spontaneously tilts all the way to touch the electrode.
21. In the bridge circuit, ac excitations of opposite phases are applied to the two bottom electrodes. The top plate is connected to the input of a charge preamplifier that is a virtual ground. The output of the charge preamplifier is fed into the input of a lockin amplifier. When the sphere is far from the top plate, the amplitudes of the ac excitations are adjusted so that the output of the pre-amplifier is zero. As the sphere approaches and the plate rotates in response to the attractive force, the capacitance of the top plate to the two electrodes changes and the bridge goes out of balance. The lockin output is thus proportional to the rotation of the top plate.
22. Rotation of the top plate in response to the attractive force reduces the separation between the sphere and the plate. To calculate the correction to the distance due to rotation of the plate, we extend the piezo until the sphere and the plate come into contact. As we further extend the piezo, the top plate rotates by a known amount and we record the corresponding change in the capacitance signal of the torsional device. This calibrates the capacitance change with respect to the rotation of the plate. In measuring the electrostatic force and Casimir force, we retract the piezo until the sphere separates from the plate and then reapproach the sphere to the desired distance from the top plate. From the capacitance signal, we calculate the rotation of the plate in response to the attractive force and subtract this amount from the separation between the sphere and the plate.
23. The Casimir force is negligible compared with the electrostatic force ($V = 289$ mV) at distances larger than 300 nm but increases rapidly at small distances. At the smallest separations (~70 nm), the Casimir force is responsible for producing up to 10% of the total rotation angle. In Fig. 2, the contributions of the Casimir force (the measurement of which is described later in the text) to the rotation angle have been subtracted, yielding the rotation produced solely by the electrostatic force. Performing this procedure increases the fitted value of z_o by ~7 nm. The validity of this procedure is justified by the consistency of the fitting results when different voltages are applied to the sphere in the electrostatic force measurement.
24. E. D. Palik, Ed., *Handbook of Optical Constants of Solids* (McGraw-Hill, New York, 1950).
25. E. M. Lifshitz, *Sov. Phys. JETP* **2**, 73 (1956).
26. S. L. Lamoreaux, *Phys. Rev. A* **59**, 3149 (1999).
27. ———, *Phys. Rev. Lett.* **83**, 3340 (1999).
28. H. G. Craighead, *Science* **290**, 1532 (2000).
29. We thank M. Schaden, L. Spruch, M. R. Andrews, D. Abusch-Magder, E. K. Chan, R. de Picciotto, C. F. Gmachl, L. N. Pfeiffer, P. M. Platzman, and N. Zhitenev for assistance and useful discussions.

Spherical Bilayer Vesicles of Fullerene-Based Surfactants in Water: A Laser Light Scattering Study

Shuiqin Zhou,[1] Christian Burger,[1] Benjamin Chu,[1]*
Masaya Sawamura,[2] Noriaki Nagahama,[2] Motoki Toganoh,[2]
Ulrich E. Hackler,[2] Hiroyuki Isobe,[2] Eiichi Nakamura[2]

The low solubility of fullerenes in aqueous solution limits their applications in biology. By appropriate substitution, the fullerenes can be transformed into stabilized anions that are water soluble and can form large aggregated structures. A laser light scattering study of the association behavior of the potassium salt of pentaphenyl fullerene ($Ph_5C_{60}K$) in water revealed that the hydrocarbon anions $Ph_5C_{60}^-$ associate into bilayers, forming stable spherical vesicles with an average hydrodynamic radius and a radius of gyration of about 17 nanometers at a very low critical aggregation concentration of less than 10^{-7} moles per liter. The average aggregation number of associated particles in these large spherical vesicles is about 1.2×10^4.

The extremely hydrophobic C_{60} fullerene can be made soluble in water by connecting it with functional chargeable groups such as carboxylic acids (*1–5*) or amines (*6–8*). Hydrophilic behavior can also be introduced by an elegant and less obvious approach, one in which polarizable phenyl groups are added to C_{60} to stabilize its anion (*9–12*). Because these compounds are composed solely of carbon and hydrogen atoms, they represent a rare example of a hydrophobic hydrocarbon ball linked to a hydrophilic ion, causing the penta-substituted fullerene to achieve a surfactant functionality, as shown schematically in Fig. 1, that is different from whole-lipid substituents (*13*). The cyclopentadienide anion has intrinsic high stability through delocalization of the negative charge toward the 50-π electron system at the bottom of the C_{60} cage. This occurs as a result of "endohedral homoconjugation" (*14*) rather than by steric protection of the cyclopentadienide anion by the phenyl substituents against the attack of water or protons (i.e., kinetic stability).

We conducted a laser light scattering (LLS) study of the association behavior of $Ph_5C_{60}K$ in water. By using a combination of static and dynamic light scattering measure-

ments, we have determined the size of $Ph_5C_{60}K$ (in terms of both the radius of gyration and the hydrodynamic radius), the size distribution, and the shape of the associated particles. We also estimated the critical aggregation concentration and the average aggregation number of the aggregated particles. A model for the resulting aggregates is presented.

The cyclopentadienides are readily available through the fivefold addition of organocopper reagent to C_{60} (*9–12*). A tetrahydrofuran (THF)-free aqueous solution of the fullerene cyclopentadienide was prepared under argon atmosphere by addition of a portion of the dark red THF solution of $Ph_5C_{60}K$ (3×10^{-3} mol liter^{-1}) into ultrapure water (THF:water ratio = 1:10 by volume), followed by evaporation of THF and repetition of this cycle four times. At concentrations of $C \geq 5 \times 10^{-3}$ mol liter^{-1}, a phase separation occurred, showing a turbid sample with visible solid particles so that no light scattering experiments could be carried out. At a concentration of $C = 2 \times 10^{-3}$ mol liter^{-1}, only a small amount of precipitation occurred and was removed by centrifugation (10 min at 1.5×10^4 rpm), leading to a dark red–colored clear stock solution that was used for the light scattering experiments.

A standard laboratory-built LLS spectrometer equipped with a BI-9000AT digital correlator (Brookhaven Instruments) and a Coherent diode-pumped solid-state (DPSS) model 532 laser operating at 200

[1]Department of Chemistry, State University of New York, Stony Brook, NY 11794, USA. [2]Department of Chemistry, University of Tokyo, Hongo, Bunkyo-ku, Tokyo 113-0033, Japan.

*To whom correspondence should be addressed. E-mail: bchu@notes.cc.sunysb.edu